Electrical properties of $Ca_{3-x}Sm_xCo_4O_{9+\delta}$ ceramics prepared under magnetic field*

Xiu-Rong Qu(曲秀荣)[1,2,†], Yan-Yan Xu(徐岩岩)[1], Shu-Chen Lü(吕树臣)[1], and Jian-Min Hu(胡建民)[1]

[1] *Key Laboratory of Photonic and Electric Bandgap Materials, and School of Physics and Electronic Engineering, Harbin Normal University, Harbin* 150025, *China*

[2] *School of Materials Science and Engineering, Dalian University of Technology, Dalian* 116024, *China*

(Received 17 August 2019; revised manuscript received 1 February 2020; accepted manuscript online 13 February 2020)

We fabricate Sm-doped $Ca_3Co_4O_{9+\delta}$ (CCO) bulk materials in magnetic field during both processes of chemical synthesis and cold pressing. The structure and electrical performance of the samples are investigated. With the increasing Sm concentration, the electrical conductivity $1/\rho$ decreases and the Seebeck coefficient α increases. As a result, the power factor ($PF = \alpha^2/\rho$) is raised slightly. After applying magnetic field, the extent of texture, grain size and density of all the bulk materials are improved obviously, thereby an enhanced electrical conductivity can be gained. Additionally, the degeneracy of Co^{4+} state in the CoO_2 layer of CCO is also increased as the magnetic field is used in the preparing process, which results in an enhanced α. The $Ca_{2.85}Sm_{0.15}Co_4O_{9+\delta}$ prepared in magnetic field shows the largest power factor (0.20 $mW{\cdot}m^{-1}{\cdot}K^{-2}$ at 1073 K).

Keywords: chemical preparation, magnetic field, structure, electrical characteristic

PACS: 61.72.S–, 63.22.Np, 72.15.Jf **DOI:** 10.1088/1674-1056/ab75cb

1. Introduction

As a functional material used for the conversion between thermal and electric energy, thermoelectric materials are investigated widely.[1–4] The electrical transport is usually evaluated by the power factor α^2/ρ, where α and ρ are the Seebeck coefficient and the electrical resistivity, respectively.[5]

$Ca_3Co_4O_{9+\delta}$ has attracted continuous attention because of both the coexisting high Seebeck coefficient and thermal stability.[6] The CCO is composed of two misfit-layered subsystems of CoO_2 layer and Ca_2CoO_3 layer along the c axis.[7] Co^{3+} and Co^{4+} have three kinds of spin states, respectively, including low spin state (LS), intermediate-spin state (IS) and high spin state (HS).[8] The special structure as described above makes it possible to optimize electrical conductivity and Seebeck coefficient simultaneously.[9]

The rare earth substitutions at Ca-sites are effective in improving the Seebeck coefficient α. For instance, Nong *et al.* reported that the α values of CCO can be enhanced significantly by rare earth substitution at Ca-site, such as Lu, Dy and Ho.[10]

Wang *et al.* reported that Sm doping can effectively improve thermoelectric properties of CCO materials.[11] The substitutions of the high valence ions for calcium sites may improve α from the reduced number p of holes in p-type semiconductor. To consider the similar ionic radius and average higher valence between Sm ions and Ca ions, we choose to utilize Sm elements to substitute Ca sites.

The misfit layered structure of CCO shows highly anisotropic properties, which leads to high resistivity for randomly oriented poly-crystalline materials. To decrease resistivity, many efforts have been taken to enhancement of the textured degree. Most of them improve the textured extent of ceramic materials by spark plasma sintering or hot pressing.[12,13] Additionally, Torres and Chen *et al.* have gained textured CCO materials by reducing the sizes of precursor powders.[14,15] Recently, more and more attentions focus on tuning physical properties of materials by inducing magnetic field in prepared process. Due to the CCO's magnetic anisotropy and the coexistence of different spin states, applying uniform magnetic field is more helpful to form textures. Huang *et al.* reported that the textured degree of CCO can be obviously improved by applying high magnetic field (4 T and 8 T) in the sample sintering process.[9] However, in such a strong magnetic field environment it is difficult to obtain CCO generally and the cost is expensive. Several reports have described that the textures may be produced and the spin can reorient by inducing weaker magnetic field during the process of chemical reaction.[16,17] For example, Du *et al.*[18] synthesized Fe_3O_4 nanoparticles with orderly arrangement under 0.4 T magnetic field. In addition, the defect splitting and electron pumping towards higher energy level can happen as magnetic field reach 0.1 T in CCO materials.[19]

Therefore, we prepared the precursor powders of $Ca_{3-x}Sm_xCo_4O_{9+\delta}$ firstly by sol-gel method under 0.5 T uniform magnetic field. Secondly, the CCO powders were cold pressed to pellets in 0.3 T uniform magnetic field. Finally, the above pellets were further hot-pressed and sintered. The effects of Sm doping and magnetic field utilizing on the struc-

*Project supported by the National Natural Science Foundation of China (Grant No. 51302055).

†Corresponding author. E-mail: quxiurong2002@163.com

ture and electric properties of CCO ceramics are studied in detail.

2. Experimental procedure

To synthesize $Ca_{3-x}Sm_xCo_4O_{9+\delta}$ powders, we used distilled water to dissolve nitrates of Ca, Sm and Co. Drop 1 mol/l citric acid into the above nitrate solution slowly until the pH value equals 2. In 0.5 T magnetic field, the above mixed liquid was stirred at 353 K until forming colloid, and then the colloid was dried. To decompose the organic molecules and nitrates, the dry gel was burned by self-propagating method. The precursor was annealed for 6 h at 1073 K to form CCO powders. The grinding CCO powders were cold pressed firstly in magnetic field (0.3 T). The dense CCO bulks were prepared by further hot-pressing at 493 K for 1.5 h (40 MPa), and then sintering at 1123 K for 12 h. For convenience, the $x = 0$–0.25 Sm-doped samples are named as CCO, CSCO5, CSCO10, CSCO15 and CSCO25, and the corresponding samples prepared under magnetic field are named as CCOM, CSCO5M, CSCO10M, CSCO15M and CSCO25M, respectively.

The crystal structure of the synthesized $Ca_{3-x}Sm_xCo_4O_{9+\delta}$ samples was measured (Fig. 1(a)) by an x-ray diffractometer (Rigaku, D/MAX 2200). Cu $K\alpha$ radiation is used at 40 kV and 100 mA. X-ray photoelectron spectroscopy (XPS) measurements were performed on a KRATOS (Axis Ultra^{DLD}) electron spectrometer at a base pressure of 9.8×10^{-10} Torr using Al $K\alpha$ radiation ($h\nu = 1486.6$ eV).

The morphological characteristics were tested by a scanning electron microscope (SU-70), and the energy dispersed spectrum (EDS) was measured. We measured the density using the Archimedes principle. The samples with the size of 13 mm × 2 mm ×2 mm were used for testing resistivity, which were carried using the conventional DC four-probe method (Fig. 1(b)). According to the relation $\alpha = \Delta E/\Delta T$, α values were obtained by testing the thermal voltage ΔE and the temperature difference ΔT through the bar bulk as shown in Fig. 1(c). We simultaneously measured α and ρ in quartz protection tube. At room temperature, the amount of hole p and mobility μ were determined by Hall instrument (HL5500PC). The used four-probe method is shown in Fig. 1(d).

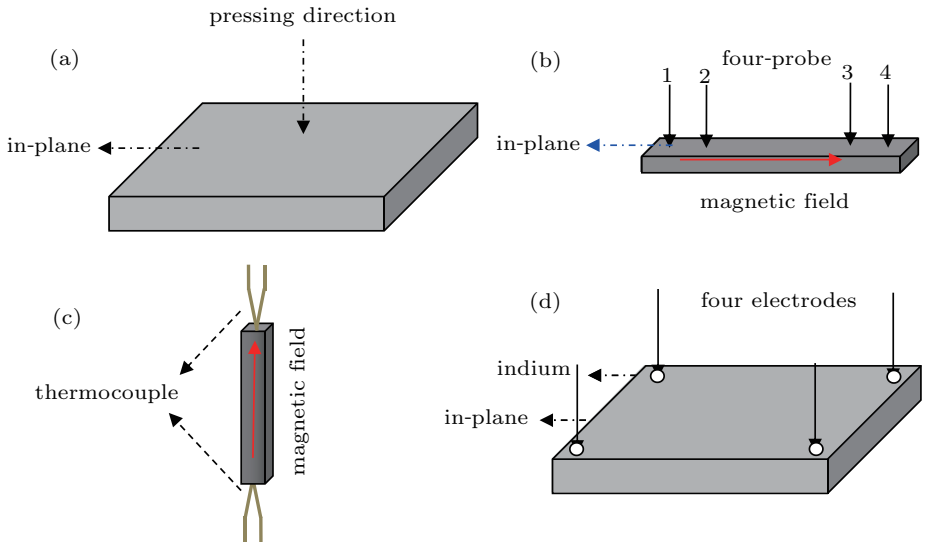

Fig. 1. Schematic diagrams of the samples for the measurements of (a) x-ray diffraction, (b) electric resistivity, (c) Seebeck coefficient, and (d) Hall coefficient.

3. Results and discussion

The x-ray diffraction patterns of the Sm-doped samples are presented in Fig. 2(a). As $x \leq 0.15$, only $CaCo_4O_{9+\delta}$ (PDF#21-0139) phase was detected, which is in agreement with Ref. [20]. With further increase of x to 0.25, weak Sm_2O_3 peaks (PDF#43-1029) can be observed (Fig. 2(b)). As displayed in Fig. 2(c), a small shift towards lower 2θ angle appears with the increasing Sm concentration from 0 to 0.15, which suggests that Sm ions with average larger radii substitute Ca sites (reference Bragg equation $2d \sin\theta = n\lambda$). As well known, Sm^{2+} (1.22 Å) is larger and Sm^{3+} (0.96 Å) is smaller compared with Ca^{2+} (0.99 Å). Thus, as $x \leq 0.15$, more Sm^{2+} with larger radius occupied Ca-sites. Increasing x from 0.15 to 0.25, the peaks shift towards higher angles, which is attributed to the fact that more and more Sm^{3+} ions substitute Ca sites. This will be further discussed in XPS part (Fig. 3). The peaks shift towards lower angles from the samples obtained under external magnetic field, which mostly results from the different radii of cobalt ions as analyzed in Ref. [21].

Table 1 shows the lattice parameters of Sm-doped samples obtained by the least-square method.[22] With the increasing Sm concentration, the lattice parameters increase slightly due to larger ionic radii of Sm^{2+} than that of Ca^{2+}. Compared with the CSCO15 (M) samples, with further increase of x to 0.25, the lattice parameters decrease conversely. In addition, the lattice parameters also increase with using external magnetic field.

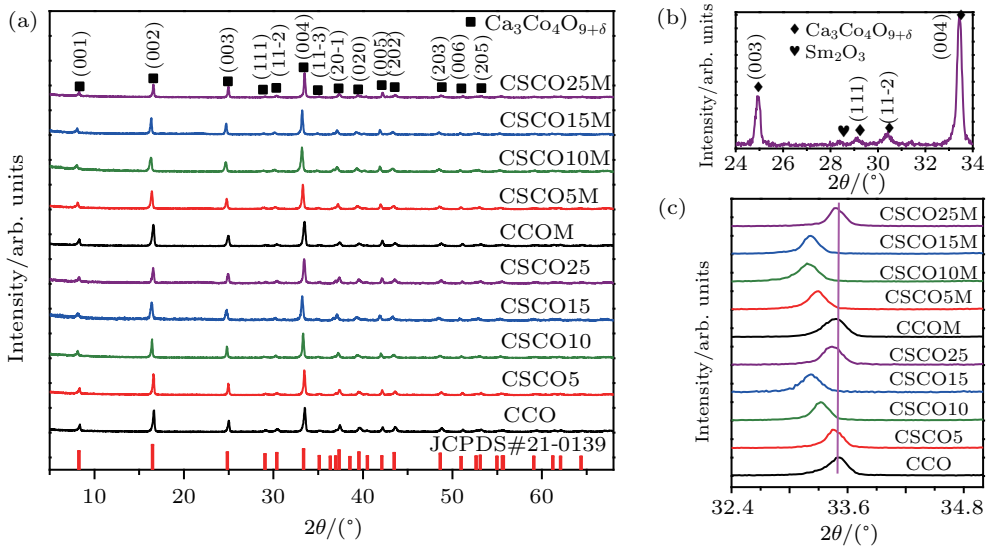

Fig. 2. (a) XRD patterns of Sm-doped bulk materials, (b) the enlarged partial diffraction peaks of the CSCO25 sample, (c) the enlarged (004) diffraction peaks of the samples studied.

Table 1. Summaries of lattice parameters, Lotgering factor F and relative density (RD) of the Sm-doped samples.

Samples	Composition	Abbreviation	a/Å	b/Å	c/Å	β/(°)	F	RD/%
Without magnetic field	$Ca_3Co_4O_{9+\delta}$	CCO	4.8232	4.5406	10.7739	98.0025	0.496	87.65
	$Ca_{2.95}Sm_{0.05}Co_4O_{9+\delta}$	CSCO5	4.8293	4.5569	10.7823	98.1932	0.462	81.38
	$Ca_{2.90}Sm_{0.10}Co_4O_{9+\delta}$	CSCO10	4.8429	4.5702	10.8871	98.2004	0.424	79.96
	$Ca_{2.85}Sm_{0.15}Co_4O_{9+\delta}$	CSCO15	4.8436	4.5769	10.9304	98.3475	0.386	77.53
	$Ca_{2.75}Sm_{0.25}Co_4O_{9+\delta}$	CSCO25	4.8234	4.5635	10.7783	98.0468	0.307	75.51
With magnetic field	$Ca_3Co_4O_{9+\delta}$	CCOM	4.8236	4.5411	10.7816	98.0085	0.513	92.71
	$Ca_{2.95}Sm_{0.05}Co_4O_{9+\delta}$	CSCO5M	4.8338	4.5600	10.9039	98.3474	0.497	86.44
	$Ca_{2.90}Sm_{0.10}Co_4O_{9+\delta}$	CSCO10M	4.8816	4.5746	10.9905	99.0365	0.487	81.58
	$Ca_{2.85}Sm_{0.15}Co_4O_{9+\delta}$	CSCO15M	4.8890	4.5882	11.0766	99.2068	0.474	79.35
	$Ca_{2.75}Sm_{0.25}Co_4O_{9+\delta}$	CSCO25M	4.8298	4.5680	10.7919	98.0701	0.461	78.14

Lotgering factor F was explored on that basis of x-ray diffraction data, which was summarized in Table 1. Generally, F was expressed as $F = (P - P_0)/(1 - P_0)$, $P = \Sigma I(00l)/\Sigma I(hkl)$. Here P is counted from the prepared samples and P_0 is obtained from the standard card.[23] Obviously, the F values for the bulks prepared in magnetic field are larger. With the increasing Sm doping concentration, the degree of textures decreases.

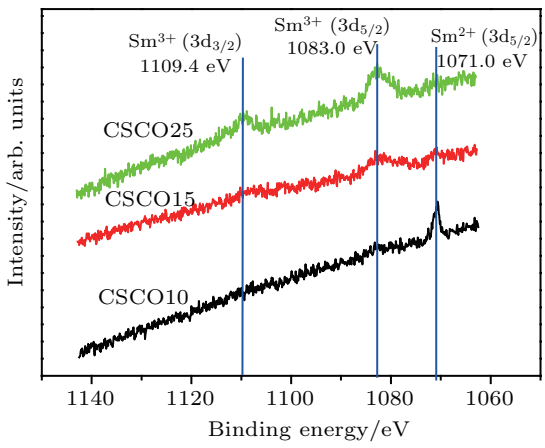

Fig. 3. XPS spectra of Sm 3d of CSCO10, CSCO15 and CSCO25.

The interest to the samarium compounds gives rise due to the existence of mixed valence state of samarium ions. According to Brunckova *et al.*,[24] the XPS spectrum of Sm 3d consists two components related to Sm^{3+} ($4f^5$) and Sm^{2+}($4f^6$). To identify the valence state of samarium ions, the XPS investigation is carried out. For the $x = 0.05$ sample, the Sm concentration is too low to identify the diffraction peaks of Sm ions. Thus, the XPS spectra of the $Ca_{3-x}Sm_xCo_4O_{9+\delta}$ ($x = 0.1$–0.25) samples are given in Fig. 3. For the $x = 0.1$ sample (CSCO10), only the strongest peak of Sm^{2+} ($3d_{5/2}$) located at about 1071.0 eV is observed.[24,25] As $x = 0.15$, the peak of Sm^{2+} ($3d_{5/2}$) has dropped and the strongest peak of the Sm^{3+} component located at 1083.0 eV ($3d_{5/2}$) is identified clearly. With further increase of x to 0.25, the peak of Sm^{2+} ($3d_{5/2}$) nearly disappears and the doublet of the Sm^{3+} component located at 1083.0 eV ($3d_{5/2}$) and 1109.4 eV ($3d_{3/2}$) is detected obviously.[24–26] The Sm 3d states are split into two lines Sm $3d_{5/2}$-Sm $3d_{3/2}$ with energy difference 26.4 eV, which is due to the spin orbit interaction. Thus, as $x = 0.1$, Sm^{2+} is the dominant substituted component at Ca^{2+} site. With the increasing Sm concentration x from 0.15 to 0.25, more and more Sm^{3+} ions substitute for Ca^{2+} ions. The re-

sults are well in accord with the analysis of previous XRD and lateral holes concentration data.

Figure 4 gives the fractured scanning pictures of the $Ca_{3-x}Sm_xCo_4O_{9+\delta}$ samples. Due to the CCO's layer-structural feature, laminated microstructure is clearly seen as shown in Figs. 4(a)–4(g). With the increasing x, less laminated structures are observed, and the average crystal size decreases (CCO: 1–2 μm; CSCO5: ∼1 μm; CSCO15: ∼0.8 μm). In the samples prepared under magnetic field, the degree of orientation and grain sizes are increased obviously. Table 1 also gives the relative densities. When taking theoretical density as 4.94 g/cm^3, the relative densities of the samples rang from 87.65% to 75.51% with the increasing Sm concentrations x from 0 to 0.25. However, relative densities of the bulk ceramics prepared in magnetic field are larger. The EDS (Fig. 4(h)) displays that the Sm-doped sample has all the expected elements. The quantitative analysis of the spectrum reveals that the atomic ratio of the bulk is very close to the (Ca + Sm):Co:O = 9:12:28 (the inset in Fig. 4(h)).

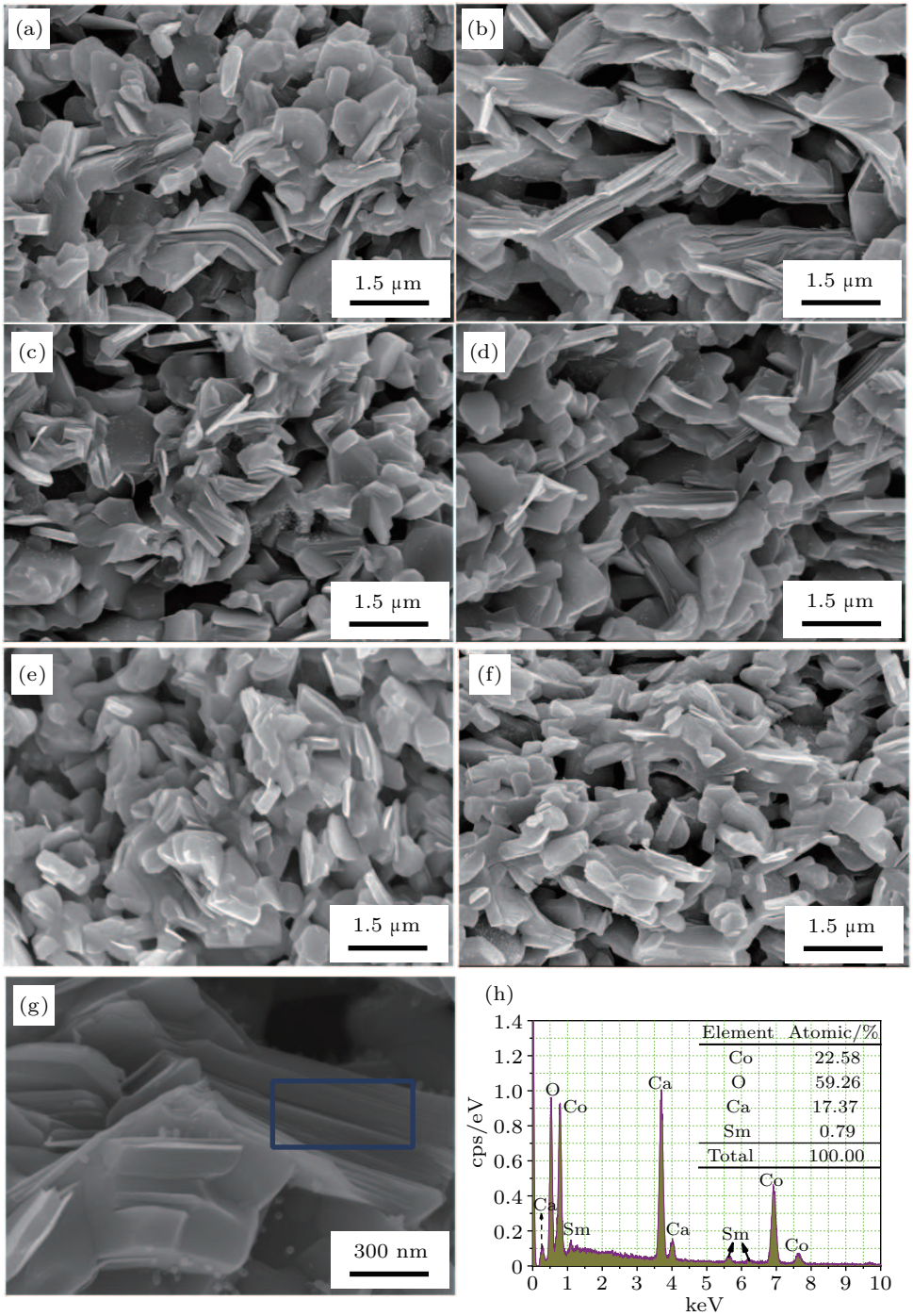

Fig. 4. Fractured cross-sectional SEM images of bulk materials: (a) CCO, (b) CCOM, (c) CSCO5, (d) CSCO5M, (e) CSCO15, (f) CSCO15M, (g) CSCO15, and (h) EDS of CSCO15.

The electrical resistivity ρ of $Ca_{3-x}Sm_xCo_4O_{9+\delta}$ bulk materials is plotted in Fig. 5(a). With the increasing Sm concentration, the ρ increases monotonously. The ρ can be described by $1/\rho = pe\mu$,[27] where p is the amount of holes and μ is mobility. Thus, the increase of ρ with the increasing x is mainly from the decrease of both the p and μ (Figs. 5(b) and 5(c)). With Sm increasing, the decrease of p means that Sm^{3+} has partly substituted Ca ions. The reduction of μ is owed to the declines in texture, relative density and grain size. Thus, the increase of ρ comes from the combined effects among the holes concentration, grain size, density and extent of texture. Compared with other lanthanide components, Sm doping has almost the same influence on the ρ of CCO ceramic materials.[10] However, the ρ values for the bulk materials fabricated in magnetic field are smaller. For example, at 323 K, the $\rho = 15.56$ mΩ·cm (CSCO15M) is much lower than that of CSCO15 ($\rho = 19.42$ mΩ·cm).

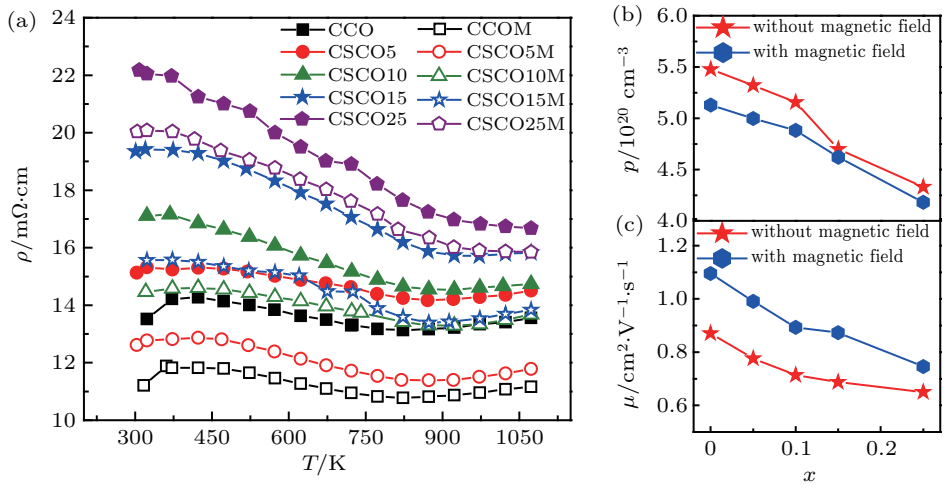

Fig. 5. Electrical properties of Sm-doped CCO: (a) electrical resistivity ρ versus temperature T, (b) and (c) relationship of hole concentration p and mobility μ with doping amount x.

Figure 6 gives the changes of $\ln(T/\rho)$ with $1000/T$ of $Ca_{3-x}Sm_xCo_4O_{9+\delta}$. As $T > 673$ K, the CCO system complies with the small polaron hopping conduction (SPHC) model, which is in agreement with Ref. [28]. According to the SPHC model, the resistivity ρ is depressed as functions of hole concentration p, activation energy E_a and temperature T:[27]

$$\frac{1}{\rho} = pea^2\left(\frac{A}{T}\right)\exp\left(\frac{-E_a}{k_B T}\right), \tag{1}$$

where e, a, A, and k_B are the absolute value of electron charge, intersite distance of hoping, pre-exponential term, and Boltzmann constant, respectively. The E_a curves are determined by the slopes of the $\ln(T/\rho)$ versus $1000/T$ curves.

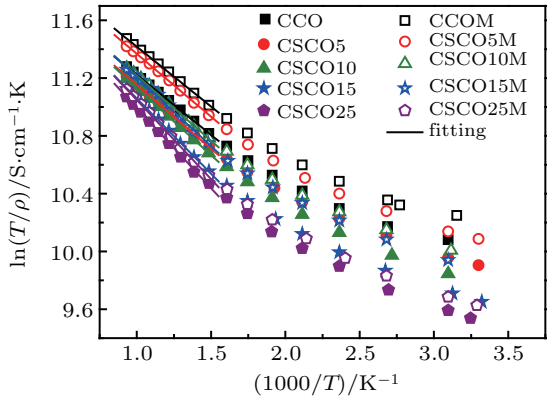

Fig. 6. Changes of $\ln(T/\rho)$ with $1000/T$ for Sm-doped bulk materials.

Figure 7 shows the change of activation energy versus the Sm concentration, and the temperature range is 673–1073 K. The activation energy increases from 70.87 meV to 94.57 meV with increasing x from 0 to 0.15, which is due to the fact that Sm impurities in the Ca_2CoO_3 layer would disturb the conduction route. On the other hand, the activation energy reduces slightly with using external magnetic field, which is mainly from the energy that has been stored in the samples during the preparing process.

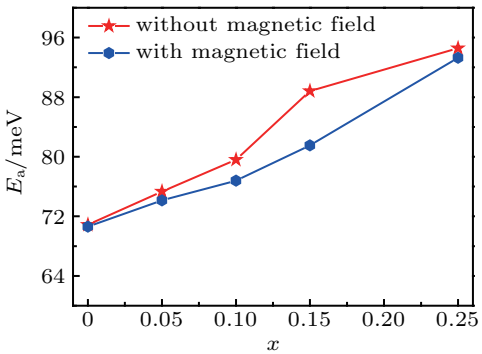

Fig. 7. Variations of activation energy with the Sm-doping content.

Figure 8 gives the Seebeck coefficient α of the Sm-doped samples. The specimens show positive α values, confirming the p-type semiconductor behavior. The α increases from 109.9 μV/K (CCO) to 136.3 μV/K (CSCO15) at 423 K. According to the Mott formula,[29] α of the CCO system is de-

scribed by the amount of hole p,

$$\alpha = \frac{C_e}{p} + \frac{\pi^2 k_B T}{3e}\left[\frac{\partial \ln \mu(\varepsilon)}{\partial \varepsilon}\right]_{\varepsilon=E_F}, \quad (2)$$

where C_e and $\mu(\varepsilon)$ are electronic specific heat and energy correlated carrier mobility. In the CCO system, α depends mainly on the hole concentration according to the simple Drude model $\alpha \sim C_e/p$.[30] Therefore, the increase of α is due to the reduction in p. In addition, the lower density and smaller grain size could increase grain boundary scattering, which also makes α values improve. Still, α values in CSCO25 are smaller than those in CSCO15 because of the impure Sm_2O_3 phase, as shown in Fig. 2(b). The impact trend of Sm doping and the α values are also similar to other CCO materials doped with rare earth ions such as La, Pr and Lu.[10,30] However, the applying of external magnetic field can not change the shapes of the $\alpha(T)$ slope but improves α values. For instance, at 423 K, the $\alpha = 146.3$ μV/K (CSCO15M) is much larger than the $\alpha = 136.3$ μV/K (CSCO15). The increase of α values is considered to be from the change of degeneracy and ratio of Co^{3+} and Co^{4+}.

In the $Ca_3Co_4O_{9+\delta}$ system, α may be expressed by the modified Heikes equation:[31]

$$\alpha = -\frac{k_B}{e}\ln\left[\frac{g_3}{g_4}\left(\frac{x}{1-x}\right)\right], \quad (3)$$

where g_3 and g_4 represent the spin-orbital degeneracies of Co^{3+} and Co^{4+} ions in the CoO_2 layers, and x is the amount of Co^{4+}. It is reported that the number of Co^{4+} in $Ca_3Co_4O_{9+\delta}$ is not changed by external magnetic field.[9] In other words, the x value is unchanged with applying magnetic field. Thus, the improvement of α is largely because of the increase of the Co ions' degeneracy. As we reported in Ref. [32], with adding external magnetic field, partial electrons in t_{2g} orbital can leap to higher e_g level. As reported in Ref. [9], the electron leaping behavior is more easily to occur in Co^{4+} ions compared with Co^{3+} ions. Thus, the improvment of the α coefficient is mainly from the increase of the g_4 in the system.

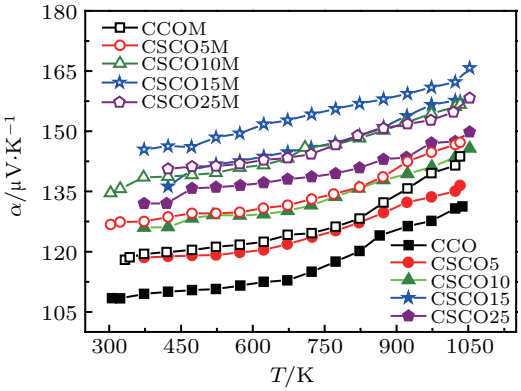

Fig. 8. Changes of Seebeck coefficient α with temperature.

The power factor PF for all the specimens increases with temperature because of the enhancement in both $1/\rho$ and α (Fig. 9). It shows that Sm-doping can evidently enhance PF, especially at higher temperatures. For example, at 1073 K, the PF of CSCO15 could reach up to 0.16 $mW{\cdot}m^{-1}{\cdot}K^{-2}$, which exceeds 23.86% compared with CCO. The result is well accord with the report by Wang *et al.*[11] Applying external magnetic field can cause significant increases in the both $1/\rho$ and α, therefore the PF is improved remarkably. Among all the Sm-doped series, CSCO15M has the largest PF value (0.20 $mW{\cdot}m^{-1}{\cdot}K^{-2}$ at 1073 K). The conclusion agrees with the report by Huang *et al.*[9] However, Huang *et al.* mainly studied the effects of magnetic field in the sample sintering process on the thermoelectric properties of CCO in the temperature range of 2–350 K.

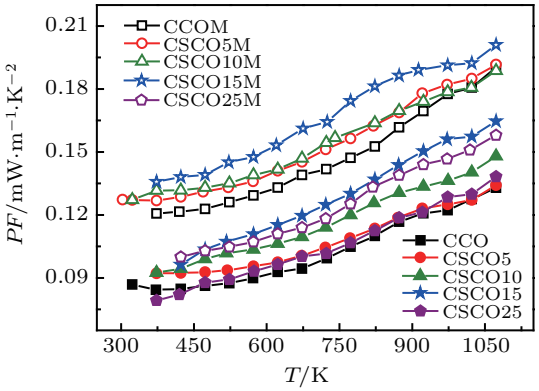

Fig. 9. Changes of power factor with temperature.

4. Conclusions

$Ca_{3-x}Sm_xCo_4O_{9+\delta}$ bulk materials with high orientation have been obtained by the inducement of magnetic field, and the structure and electrical performance are studied in detail. The results show that samarium doping can cut down the texture and the number of the holes. Thus, the $1/\rho$ decreases and α increases, which results in high PF. Utilizing magnetic field to synthesize $Ca_{3-x}Sm_xCo_4O_{9+\delta}$ bulk materials can improve the PF effectively. The present study describes that the electrical properties of $Ca_3Co_4O_{9+\delta}$ can be enhanced by applying magnetic field and doping samarium.

References

[1] Wu H, Shaheen N, Yang H Q, Peng K L, Shen X C, Wang G Y, Lu X and Zhou X Y 2018 *Chin. Phys. B* **27** 047203
[2] Ahmad K, Wan C, Al-Eshaikh M A and Kadachi A N 2019 *Appl. Surf. Sci.* **474** 2
[3] Liu C Y, Miao L, Wang X Y, Wu S H, Zheng Y Y, Deng Z Y, Chen Y L, Wang G W and Zhou X Y 2018 *Chin. Phys. B* **27** 047211
[4] Wang H, Chen J, Lu T Q, Zhu K J, Li S, Liu J and Zhao H Z 2018 *Chin. Phys. B* **27** 047212
[5] Jiang G Y, He J, Zhu T J, Fu C G, Liu X H, Hu L P and Zhao X B 2014 *Adv. Funct. Mater.* **24** 3776
[6] Li Y N, Wu P, Zhang S P, Chen S, Yan D, Yang J G, Wang L and Huai X L 2018 *Chin. Phys. B* **27** 057201

[7] Klie P F, Qiao Q, Paulauskas T, Gulec A, Rebola A and Öğüt S 2012 *Phys. Rev. Lett.* **108** 196601
[8] Soret J and Lepetit M B 2012 *Phys. Rev. B* **85** 165145
[9] Huang Y N, Zhao B C, Fang J, Ang R and Sun Y P 2011 *J. Appl. Phys.* **110** 123713
[10] Nong N V, Liu C J and Ohtaki M 2011 *J. Alloy Compd.* **509** 977
[11] Wang D L, Chen L D, Bai S Q and Li J G 2004 *J. Inorg. Mater.* **19** 1329 (in Chinese)
[12] Noudem J G 2009 *J. Eur. Ceram. Soc.* **29** 2659
[13] Lim C Y, Seo W S, Lee S, Lim Y S, Kim J Y, Park H H, Chol S M, Lee K H and Park K 2015 *J. Korean Phys. Soc.* **66** 794
[14] Torres M A, Garcia G, Urrutibeascoa I, Madre M A, Diez J C and Sotelo A 2019 *Sci. Chin. Mater.* **62** 399
[15] Chen S, Song X Y, Chen X Q, Chen Y, Barbero E J, Thomas E L and Narnes P N 2007 *Ceram. Int.* **33** 1305
[16] Zhao X B, Pang Z W, Wu M Z, Liu X S, Zhang H, Ma Y Q, Sun Z Q, Zhang L D and Chen X S 2013 *Mater. Res. Bull.* **48** 92
[17] Gnatchenko S L, Chizhik A B, Merenkov D N, Eremenko V V, Szymczak H, Szymczak R, Fronc K and Zuberek R 1998 *J. Magn. Magn. Mater.* **186** 139
[18] Du M, Cao X Z, Xia R, Zhou Z P, Jin S X and Wang B Y 2019 *Chin. Phys. B* **28** 027805
[19] Huang K and Han R Q 1988 *Solid State Physics* (Beijing: Higher Education Press) pp. 394–395
[20] Nong N V, Pryds N, Linderoth S and Ohtaki M 2011 *Adv. Mater.* **23** 2484
[21] Xu Y Y, Qu X R, Lü S C, Qian Y, Hu J M and Meng Q Y 2016 *Ceram. Int.* **42** 6107
[22] Zhang Q L, Wang Y S, Xiao J, Li D Q and Yin S T 2009 *Chin. J. Quantum Electron.* **26** 177 (in Chinese)
[23] Lotgering F K 1959 *J. Inorg. Nucl. Chem.* **9** 113
[24] Brunckova H, Kanuchova M, Kolev H, Mudra E and Medvecky L 2019 *Appl. Surf. Sci.* **473** 1
[25] Mori Y, Tanemura S, Koide S, Senzaki Y, Jin P, Kaneko K, Terai A and Nabotova-Gabin N 2003 *Appl. Surf. Sci.* **212** 38
[26] Li L, Liu X G, Noh H M, Moon B K, Choi B C and Jeong J H 2015 *Ceram. Int.* **41** 9722
[27] Bosman A J and Van Daal H J 1970 *Adv. Phys.* **19** 1
[28] Song Y, Sun Q, Zhao L R, Wang F P and Jiang Z H 2009 *Mater. Chem. Phys.* **113** 645
[29] Mott N F and Davis E A 1979 *Electronic Processes In Non-crystalline Materials* 2nd Edn. (Oxford: Clarendon Press) pp. 101–110
[30] Wang Y, Sui Y, Li F, Xu L X, Wang X J, Su W H and Liu X Y 2012 *Nano Energy.* **1** 456
[31] Chaikin P M and Beni G 1976 *Phys. Rev. B* **13** 647
[32] Xu Y Y, Qu X R, Lü S C, Bai L N and Niu L 2016 *Ceram. Int.* **42** 11404